
Flow Matching Policy with Entropy Regularization

Ting Gao¹ Stavros Orfanoudakis¹ Nan Lin¹ Elvin Isufi¹ Winnie Daamen¹ Serge Hoogendoorn¹

Abstract

Diffusion-based policies have gained significant popularity in Reinforcement Learning (RL) due to their ability to represent complex, non-Gaussian distributions. Stochastic Differential Equation (SDE)-based diffusion policies often rely on indirect entropy control due to the intractability of the exact entropy, while also suffering from computationally prohibitive policy gradients through the iterative denoising chain. To overcome these issues, we propose Flow Matching Policy with Entropy Regularization (FMER), an Ordinary Differential Equation (ODE)-based online RL framework. FMER parameterizes the policy via flow matching and samples actions along a straight probability path, motivated by optimal transport. FMER leverages the model’s generative nature to construct an advantage-weighted target velocity field from a candidate set, steering policy updates toward high-value regions. By deriving a tractable entropy objective, FMER enables principled maximum-entropy optimization for enhanced exploration. Experiments on sparse multi-goal FrankaKitchen benchmarks demonstrate that FMER outperforms state-of-the-art methods, while remaining competitive on standard MuJoCo benchmarks. Moreover, FMER reduces training time by $7\times$ compared to heavy diffusion baselines (QVPO) and 10-15% relative to efficient variants.

1. Introduction

In continuous control Reinforcement Learning (RL), standard unimodal Gaussian policies often fail to capture complex action landscapes. Many tasks exhibit multiple distinct, state-dependent high-return behaviors, necessitating policies capable of representing multi-peaked distributions (Haarnoja et al., 2017). This has motivated the development of generative policy classes that can repre-

sent rich, multimodal action distributions by transforming noise samples into actions conditioned on the state. Diffusion policies transform this via iterative denoising (Wang et al., 2024; Yang et al., 2023), often relying on simulating a reverse-time SDE. Meanwhile, Flow Matching (FM) formulations (Lipman et al., 2023; McAllister et al., 2025) provide an ODE-based alternative that learns the underlying transport by directly regressing a vector field, closely related to Continuous Normalizing Flows (Chen et al., 2018).

Diffusion policies have first gained prominence in offline RL (Wang et al., 2023; Ajay et al., 2023), typically formulated as behavior cloning of expert data. However, extending these models to online RL is non-trivial due to the absence of pre-collected expert data. Existing online approaches fall into two categories: (1) using the diffusion model purely as an approximation tool and backpropagating policy gradients through the sampling chain (Wang et al., 2024), a process that is computationally prohibitive and susceptible to high-variance gradients (Ren et al., 2025; Ding et al., 2024); (2) leveraging the generative capability to iteratively improve the policy by regressing towards high-value samples selected by a critic (Yang et al., 2023; Ding et al., 2024; Ma et al., 2025). Our work follows the second paradigm.

Despite this progress, current research primarily focuses on SDE-based policies, with limited attention given to ODE-based formulations. While SDE frameworks such as DDPM excel at approximating complex distributions, they suffer from critical limitations in the online RL context. First, their stochastic reverse process often requires many discretization steps to approximate the curved trajectories, increasing training latency. Second, stochasticity renders the exact policy entropy intractable, a problem further compounded by the non-linear transformations required for bounded-action spaces. Therefore, existing methods cannot directly optimize the maximum entropy objective and often resort to crude heuristics (e.g., uniform distribution assumptions (Ding et al., 2024)), hindering effective exploration.

In this work, we tackle these challenges by proposing FM Policy with Entropy Regularization (FMER), a framework that leverages the ODE-based FM model as its policy backbone. By adopting the Optimal Transport objective (Lipman et al., 2023), we construct straight line probability paths between the base noise and the target data. This linearity

¹Delft University of Technology, the Netherlands. Correspondence to: Ting Gao <t.gao-1@tudelft.nl>.

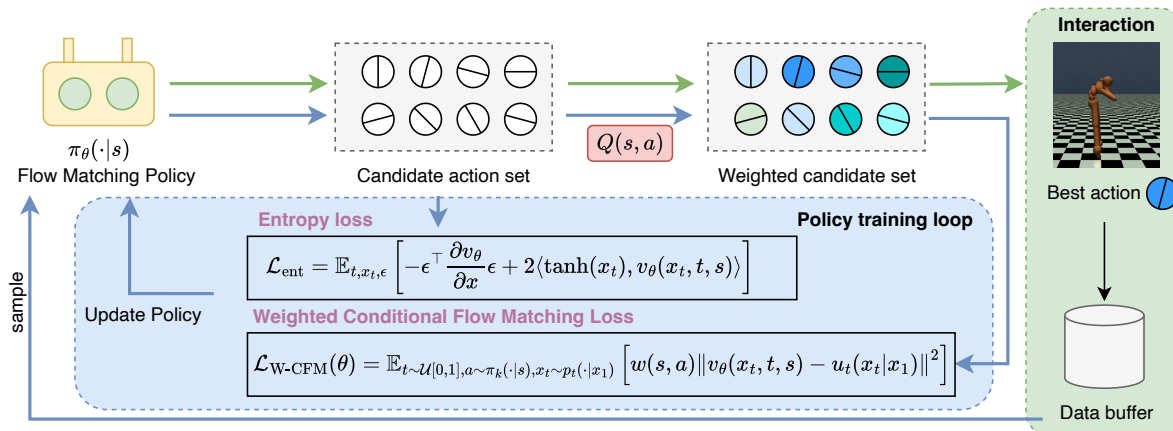


Figure 1. Overview of the FMER framework. Left (Policy Training): The policy generates a set of candidate actions, which are evaluated by the critic (Q-network) to compute advantage-based weights. These weights guide the Weighted Conditional FM loss, while an entropy regularization term ensures exploration. Right (Interaction): During data collection, the agent samples multiple candidates and executes the highest-value action to store in the replay buffer.

guarantees a deterministic sampling process while significantly reducing computational overhead. Moreover, to enhance policy exploration, we derive a tractable analytic expression for the policy entropy, enabling its direct and principled maximization. Our contributions are threefold:

- **Introduction of FMER.** We propose FMER, an RL algorithm that leverages the computational efficiency of ODE-based FM. FMER integrates an advantage-weighted regression objective to steer policy updates toward high-value regions without relying on brittle selection heuristics. Moreover, FMER utilizes direct entropy maximization to actively enhance exploration.
- **Theoretical Foundations.** We provide a theoretical proof that minimizing the Weighted Conditional FM loss is a surrogate of maximizing the lower bound of online RL objective. We also derive an analytic expression for the policy entropy, accounting for the density distortion induced by the non-linear transformation.
- **Empirical Validation.** We evaluate FMER against seven baselines (standard RL, diffusion-based RL, and flow-matching gradients) across FrankaKitchen, MuJoCo, and multi-goal environments. FMER achieves state-of-the-art returns while reducing training time by up to $7\times$ compared to heavy diffusion models (e.g., QVPO) and 10–15% relative to efficient variants.

2. Related work

Diffusion policies. Diffusion policies parameterize the policy network as a diffusion model to explicitly capture multimodal action distributions. This approach first gained prominence in the offline RL setting, adhering to the behavioral

cloning framework (Wang et al., 2023; Kang et al., 2023; Chen et al., 2023). Decision Diffuser (Ajay et al., 2023) conditions on returns to push generation toward higher-reward behavior at inference time. Extending diffusion policies to online RL has produced several lines of work: DIPO (Yang et al., 2023) updates replay actions via Q -gradients and then imitates them with a diffusion model; QSM (Psenka et al., 2024) aligns score estimates with action gradients of the critic; DACER (Wang et al., 2024) applies policy gradients through the sampling chain while approximating entropy with a Gaussian-mixture surrogate; and recent methods adopt critic-weighted regression objectives, including QVPO (Ding et al., 2024) and DPMD (Ma et al., 2025), as well as variational/inference perspectives such as DIME (Celik et al., 2025). However, many online diffusion approaches still face a trade-off between expensive, high-variance optimization through long sampling chains and heuristic target selection or approximate entropy terms that can bias exploration and destabilize improvement.

Flow Matching Policies. FM is a closely related generative formulation that replaces stochastic reverse-time dynamics with deterministic transport, learning a vector field that defines an ODE probability path (Lipman et al., 2023; Chen et al., 2018). For policies, this offers simulation-free training objectives and a deterministic sampling path that can be easier to control than diffusion denoising. FM has been explored in offline settings, e.g., SSCP (Zhang et al., 2025) proposes energy-weighted FM to learn energy-guided flows, and Rouxel et al. (2025) models goal-conditioned policies via deterministic transport. In online settings, related efforts include Flow-GRPO (Liu et al., 2025), FPO (McAllister et al., 2025) (PPO-style likelihood-ratio estimation via an FM objective), and FM-IRL (Wan et al., 2025) (teacher-student regularization for exploration). Nevertheless, com-

pared to diffusion-based online RL, FM-based policies remain less developed, and prior work typically does not focus on principled weighting and exact entropy control for off-policy critic-guided distribution shifts.

Comparison with FMER. Our method differs from previous approaches in both problem setup and technical formulation. First, we use an ODE-based FM policy and update it using a weighted candidate set rather than aggressive Top-1 regression, thereby reducing mode collapse and improving stability when the critic is imperfect. Second, we derive a closed-form entropy term that accounts for density contraction along the flow and boundary distortions induced by action squashing, avoiding the biased entropy surrogates commonly used in diffusion-based online RL and enabling direct, principled control of exploration.

3. Preliminaries

3.1. Reinforcement learning

The environment is modeled as a Markov Decision Process (MDP), defined by the tuple $(\mathcal{S}, \mathcal{A}, p, r, \rho_0, \gamma)$. Here, \mathcal{S} is the continuous state space, \mathcal{A} is the continuous action space, and the transition density $p : \mathcal{S} \times \mathcal{A} \times \mathcal{S} \rightarrow [0, \infty)$ describes the likelihood of transitioning to state s_{i+1} given action a_i in state s_i . The bounded reward function $r : \mathcal{S} \times \mathcal{A} \rightarrow \mathbb{R}$ gives a scalar reward after an action is taken. ρ_0 denotes the initial state density, and $\gamma \in [0, 1)$ is the discount factor. The RL policy is represented as $\pi(a|s) : \mathcal{S} \times \mathcal{A} \rightarrow [0, \infty)$, denoting the probability density of taking action a_i at state s_i . Starting from an initial state s_0 , the agent interacts with the environment to get a trajectory $\mathcal{T} = (s_0, a_0, r_0, s_1, \dots)$ by following the policy π . We denote the trajectory distribution induced by the policy as $\mathcal{T} \sim \rho_\pi$.

The value function $V_\pi(s) = \mathbb{E}_{\mathcal{T} \sim \rho_\pi} [\sum_{i=0}^{\infty} \gamma^i r_i \mid s_0 = s]$ estimates the expected discounted future reward starting from any given state $s_0 = s$. Similarly, the action-value function $Q_\pi(s, a) = \mathbb{E}_{\mathcal{T} \sim \rho_\pi} [\sum_{i=0}^{\infty} \gamma^i r_i \mid s_0 = s, a_0 = a]$ estimates the expected return after taking action a at state s . The advantage function $A_\pi(s, a) = Q_\pi(s, a) - V_\pi(s)$ measures the relative benefit of taking action a over the average action at state s . The goal of RL is to maximize the expected cumulative reward $J(\pi) = \mathbb{E}_{\mathcal{T} \sim \rho_\pi} [\sum_{i=0}^{\infty} \gamma^i r_i]$.

3.2. Flow Matching

Flow Matching (Lipman et al., 2023) is a generative framework that models a probability path p_t transporting a simple noise distribution p_0 (at $t = 0$) to a complex data distribution p_{data} (at $t = 1$). This transport is governed by a time-dependent ODE:

$$\frac{d}{dt} x_t = v_\theta(x_t, t), \quad (1)$$

where v_θ is a neural vector field parameterized by θ . To train this field, we define a target conditional probability path. In this work, we utilize the Optimal Transport path, which linearly interpolates between noise $x_0 \sim \mathcal{N}(0, \mathbf{I})$ and data $x_1 \sim p_{\text{data}}$: $x_t = (1 - t)x_0 + tx_1$.

This path corresponds to a conditional vector field $u_t^{\text{target}}(x_t|x_1)$ that generates the trajectory from x_0 to x_1 . For the Optimal Transport path, this vector field is the constant velocity connecting the source and target:

$$u_t^{\text{target}}(x_t|x_1) = \frac{d}{dt} x_t = x_1 - x_0. \quad (2)$$

Since the true marginal vector field is intractable, we optimize the Conditional Flow Matching (CFM) objective. As shown by Lipman et al. (2023), minimizing the CFM loss is equivalent to minimizing the intractable marginal FM loss (up to a constant):

$$\mathcal{L}_{\text{CFM}}(\theta) = \mathbb{E}_{t, x_1 \sim p_{\text{data}}, x_0 \sim p_0} \left[\left\| v_\theta(x_t, t) - u_t^{\text{target}}(x_t|x_1) \right\|^2 \right]. \quad (3)$$

4. Method

In this section, we introduce the Flow Matching Policy with Entropy Regularization (FMER) framework. Following the standard RL policy objective and the maximum entropy principle (Haarnoja et al., 2018; Peng et al., 2019), we aim to optimize the policy parameters θ to maximize the advantage-weighted log-likelihood while satisfying a minimum entropy constraint, which is equivalent to minimizing the objective:

$$\begin{aligned} \min_{\theta} \mathcal{J}(\theta) &= -\mathbb{E}_{(s,a) \sim \mathcal{D}} \left[\exp \left(\frac{A(s,a)}{\tau} \right) \log \pi_\theta(a|s) \right] \\ \text{s.t. } &\mathbb{E}_{s \sim \mathcal{D}} [\mathcal{H}(\pi_\theta(\cdot|s))] \geq \bar{H}, \end{aligned} \quad (4)$$

where \mathcal{D} is the replay buffer, τ is the temperature parameter, $\mathbb{E}_{s \sim \mathcal{D}} [\mathcal{H}(\pi_\theta(\cdot|s))]$ is the policy entropy, and \bar{H} is the target entropy. Following Haarnoja et al. (2018); Zheng et al. (2022), to avoid explicitly solving the constrained optimization, we define the Lagrangian $\mathcal{L}(\theta, \alpha)$ as:

$$\begin{aligned} \mathcal{L}(\theta, \alpha) &= -\mathbb{E}_{(s,a) \sim \mathcal{D}} \left[\exp \left(\frac{A(s,a)}{\tau} \right) \log \pi_\theta(a|s) \right] \\ &\quad + \alpha (\bar{H} - \mathbb{E}_{s \sim \mathcal{D}} [\mathcal{H}(\pi_\theta(\cdot|s))]), \end{aligned} \quad (5)$$

where $\alpha \geq 0$ is the Lagrangian multiplier.

For diffusion-based policies, directly maximizing the log-likelihood $\log \pi_\theta(a|s)$ in Eq. (5) is impractical. Computing policy gradients through the iterative denoising process is computationally prohibitive and often induces training instability (Ding et al., 2024). Similarly, exact likelihood computation requires solving an ODE during training, which

entails significant computational overhead. To address these challenges, we substitute the log-likelihood term with the Weighted Conditional Flow Matching ($\mathcal{L}_{\text{W-CFM}}$) loss, which serves as a tractable and efficient proxy. Combining this with an explicit entropy regularization term \mathcal{L}_{ent} (introduced in Sec. 4.3), we define the unified FMER loss:

$$\mathcal{L}_{\text{FMER}}(\theta) = \mathcal{L}_{\text{W-CFM}}(\theta) + \alpha \mathcal{L}_{\text{ent}}(\theta). \quad (6)$$

The Lagrangian multiplier α balances exploration and exploitation and is automatically tuned to maintain the target entropy \bar{H} following the dual gradient descent method described in Haarnoja et al. (2018).

The remainder of this section is organized as follows: Sec. 4.1 presents the policy representation, Sec. 4.2 details the $\mathcal{L}_{\text{W-CFM}}$ loss, Sec. 4.3 describes the entropy loss \mathcal{L}_{ent} , and Sec. 4.4 presents the complete training procedure. The policy training pipeline is illustrated in Figure 1.

4.1. Flow Matching Policy Representation

We parameterize the policy $\pi_\theta(a|s)$ using a Latent Conditional Flow Matching framework. We adopt this latent formulation to address the strict constraints of continuous control environments (e.g., $a \in (-1, 1)^d$). Modeling a generative flow directly in the action space risks producing out-of-bound samples due to function approximation errors or numerical drift during integration.

To resolve this, we define the flow process in an unbounded latent space, where the trajectory consists of intermediate points $x_t \in \mathbb{R}^d$ evolving from noise x_0 to a terminal latent state x_1 . The final action is then obtained via the transformation $a = \tanh(x_1)$. This formulation ensures that all generated actions are strictly valid by design. Formally, the sampled policy $a \sim \pi_\theta(\cdot|s)$ is defined as $a = \tanh(x_1)$, $x_1 \sim p_1(\cdot|s)$, where $p_1(\cdot|s)$ represents the distribution generated by the learned vector field v_θ at $t = 1$.

Network Training. When expert demonstrations are available, the policy can be trained to clone the target action distribution directly. The policy network predicts the latent vector field $v_\theta(x_t, t, s)$ and is trained to regress the target conditional vector field in the unbounded latent space. For the Optimal Transport path, the target velocity is the straight line connecting the source noise x_0 to the inverse-transformed target action $x_1 = \text{arctanh}(a)$. Given a batch of transitions (s, a) from \mathcal{D} , the loss function is:

$$\mathcal{L}_{\pi\text{-CFM}}(\theta) = \mathbb{E}_{\substack{t \sim \mathcal{U}[0,1] \\ x_0 \sim p_0 \\ (s,a) \sim \mathcal{D}}} \left[\|v_\theta(x_t, t, s) - (\text{arctanh}(a) - x_0)\|^2 \right] \quad (7)$$

where $x_t = (1-t)x_0 + tx_1$ is the linear interpolation in latent space. By minimizing this objective, the network learns to transport Gaussian noise into the latent distribution that maps to the target actions.

Policy Sampling. During inference, to generate an action, we first solve the flow ODE in the latent space starting from noise $x_0 \sim \mathcal{N}(0, \mathbf{I})$. We employ the Euler method to discretize the trajectory into N steps of size $\Delta t = 1/N$:

$$x_{t+\Delta t} = x_t + \Delta t \cdot v_\theta(x_t, t, s), \quad t \in \left\{0, \frac{1}{N}, \dots, \frac{N-1}{N}\right\}. \quad (8)$$

The resulting terminal latent state x_1 is then transformed into the executable action via $a = \tanh(x_1)$.

4.2. Policy Optimization via Weighted-CFM

In the presence of expert demonstrations drawn from an optimal policy, loss (7) could be directly employed for behavioral cloning. However, in the online RL setting, such high-quality reference actions are initially unavailable. To overcome this limitation, we leverage a learned value function Q_ψ , parameterized by ψ , to guide the policy update. As shown in Figure 1, at each training iteration k , we sample actions from the current policy π_k , evaluate them using Q_ψ , and apply advantage-based weights to the Flow Matching loss. This re-weighting mechanism effectively shifts the training target for the subsequent iteration, steering the vector field optimization toward higher Q-value regions.

Theorem 1 (Weighted Flow Matching Surrogate). For a given state s and advantage weights $w(s, a) = \exp(A(s, a)/\tau)$, let $x_1 = \text{arctanh}(a)$ be the action mapped to the unbounded latent space. Minimizing the Weighted Conditional Flow Matching loss:

$$\mathcal{L}_{\text{W-CFM}}(\theta) = \mathbb{E}_{\substack{t \sim \mathcal{U}[0,1] \\ a \sim \pi_k(\cdot|s) \\ x_0 \sim p_0}} \left[w(s, a) \|v_\theta(x_t, t, s) - (x_1 - x_0)\|^2 \right] \quad (9)$$

is a surrogate for maximizing the lower bound of the advantage-weighted policy improvement objective:

$$\mathbb{E}_{s,a \sim \pi_k(\cdot|s)} [w(s, a) \log \pi_\theta(a|s)]. \quad (10)$$

The proof is provided in the Appendix A.1. Theorem 1 establishes a formal link between the FM training objective and advantage-weighted policy improvement by transforming policy optimization into weighted vector field regression. So, $w(s, a)$ can be viewed more broadly as an importance weight that prioritizes the objective’s target distribution.

While recent diffusion-based methods (Ding et al., 2024; Ma et al., 2025) also utilize advantage information, they typically employ heuristic strategies, such as training exclusively on the single “best” candidate (Top-1 selection). As shown in Figure 2, this hard selection is overly aggressive since it can discard valuable distributional information from other high-quality actions and renders policy updates brittle to function approximation errors (e.g., critic overestimation). In contrast, FMER employs a softer weighting mechanism consistent with the advantage-weighted log-likelihood objective, which retains a broader distribution of improving

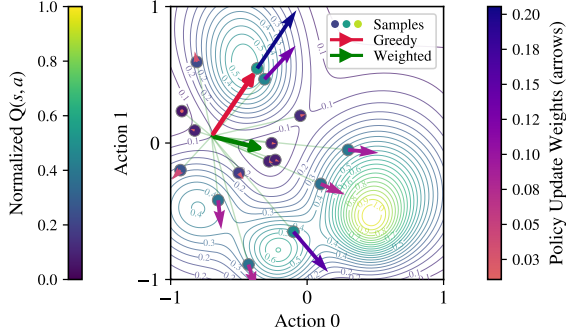


Figure 2. Weighted vs. greedy policy updates. Contours show the ground truth Q-value landscape for a fixed state. From 16 sampled candidate actions, the top-1 (greedy) update moves toward the highest-valued sample (red arrow), leading to a local maximum. In contrast, the weighted update (green) aggregates all candidates via Q-based weights (small arrows) towards the global optimal.

actions and stabilizes training against noisy value estimates. Specifically, for a set of M candidate actions $\{a^{(j)}\}_{j=1}^M$ sampled from the current policy $\pi_k(\cdot|s)$, the weight for the j -th candidate is:

$$w(s, a^{(j)}) = \frac{\exp(A(s, a^{(j)})/\tau)}{\sum_{l=1}^M \exp(A(s, a^{(l)})/\tau)}. \quad (11)$$

As illustrated in Figure 2, this soft-weighting mechanism leverages the full spectrum of candidate actions. Rather than collapsing into a single, potentially noisy target, the vector field is steered toward the high-value regions of the action space, resulting in smoother, more robust policy convergence. This design is further validated by ablation studies.

4.3. Entropy-Regularized Framework

The policy entropy in conventional diffusion-based methods, such as DDPM (Ho et al., 2020), is generally intractable due to the stochastic nature of the reverse sampling process. In contrast, the ODE-based formulation of FM allows us to explicitly track and express the policy entropy.

Theorem 2 (Entropy of Latent Flow). Consider a latent vector field $v_\theta(x, t, s)$ that transports a base distribution p_0 to the target latent distribution p_1 at $t = 1$. For the unbounded latent space \mathbb{R}^d , the entropy $H^x(p_1(\cdot|s))$ can be computed as:

$$H_1^x(p_1) = H_0^x + \int_0^1 \mathbb{E}_{x_t \sim p_t(\cdot|s)} [\nabla_x \cdot v_\theta(x_t, t, s)] dt, \quad (12)$$

where $H_0^x = \frac{d}{2}(1 + \ln(2\pi))$ is the entropy of the base Gaussian noise $p_0 = \mathcal{N}(0, \mathbf{I})$, d is the latent dimension, and $\nabla_x \cdot v_\theta = \text{Tr}(\nabla_x v_\theta)$ is the divergence of the vector field.

The proof is provided in Appendix A.2. This theorem provides a tractable mechanism to control policy exploration

directly through the vector field divergence. For practical implementation using a single-step time sample $t \sim \mathcal{U}[0, 1]$, the entropy is unbiasedly estimated by:

$$H_1^x \approx H_0^x + \mathbb{E}_{t \sim \mathcal{U}[0,1], x_t \sim p_t(\cdot|s)} [\nabla \cdot v_\theta(x_t, t, s)]. \quad (13)$$

Proposition 3 (Divergence under Tanh Transformation).

Consider the coordinate transformation $a = \tanh(x)$ mapping any latent state $x \in \mathbb{R}^d$ to the bounded action space $(-1, 1)^d$. Let $v_\theta(x, t, s)$ be the vector field in the latent space. The corresponding induced vector field in the action space, $v^a(a, t, s)$, satisfies the following divergence relationship at any point x :

$$\nabla_a \cdot v^a(a, t, s) = \nabla_x \cdot v_\theta(x, t, s) - \sum_{i=1}^d 2 \tanh(x_i) v_{\theta,i}(x, t, s), \quad (14)$$

where $v_{\theta,i}$ is the i -th component of the latent vector field.

The proof of Proposition 3 can be found in Appendix A.3. Eq. (14) allows us to optimize the action-space entropy $\pi(a|s)$ by adjusting the latent flow. To maximize entropy (minimize negative entropy), we define the entropy regularization loss \mathcal{L}_{ent} as:

$$\mathcal{L}_{\text{ent}} = -\mathbb{E}_{t, x_t} [\nabla_x \cdot v_\theta(x_t, t, s) - 2 \langle \tanh(x_t), v_\theta(x_t, t, s) \rangle]. \quad (15)$$

In practice, computing the exact divergence $\nabla_x \cdot v_\theta(x) = \sum_{i=1}^d \frac{\partial v_{\theta,i}}{\partial x_i}$ requires the trace of the Jacobian matrix, which scales as $\mathcal{O}(d^2)$ because calculating each diagonal entry of the Jacobian requires a separate differentiation pass. This quadratic complexity becomes computationally prohibitive, especially for high dimensional action spaces. To maintain efficiency, we employ Hutchinson’s trace estimator (Grathwohl et al., 2019; Hutchinson, 1989), which provides an unbiased stochastic estimate of the divergence:

$$\nabla_x \cdot v_\theta(x) = \text{Tr} \left(\frac{\partial v_\theta}{\partial x} \right) = \mathbb{E}_{p(\epsilon)} \left[\epsilon^\top \frac{\partial v_\theta}{\partial x} \epsilon \right], \quad (16)$$

where $\epsilon \in \mathbb{R}^d$ is a noise vector sampled from a distribution $p(\epsilon)$ with zero mean and unit variance. We use the Rademacher distribution as recommended by Hutchinson (1989). By leveraging modern automatic differentiation, this reduction to $\mathcal{O}(d)$ per-step complexity allows FMER to scale gracefully to complex high-dimensional environments, such as Humanoid.

Remark. Note that the Flow Matching process evolves in the unbounded latent space x , while the final policy entropy refers to the bounded action space a . The initial entropy in the action space, H_0^a , differs from the latent Gaussian entropy H_0^x by a constant Jacobian term. The final policy entropy H_1^a is obtained by evolving this base value according

Algorithm 1 Flow Matching with Entropy Regularization

- 1: **Input:** Initial parameters θ, ψ, α ; Target entropy \bar{H} ; Replay Buffer \mathcal{D} .
- 2: **for** each epoch **do**
- 3: **// Interaction**
- 4: Observe state s . Generate M candidate actions $\{a^{(j)}\}_{j=1}^M$ by solving ODE (Eq. 8). Select the best action $a = \arg \max_j Q(s, a^{(j)})$.
- 5: Execute a , observe r, s' , and store transition (s, a, r, s') in \mathcal{D} .
- 6: **// Training**
- 7: **for** K gradient steps **do**
- 8: Sample batch $B \sim \mathcal{D}$.
- 9: Critic Update: Sample M next actions via ODE solver and select the best action; compute targets y (Eq. 20). Update ψ minimizing Eq. (19).
- 10: Generate M candidate actions from $\pi_\theta(\cdot|s)$ and compute weights w via Eq. (11).
- 11: Policy Update: Sample flow time t, ϵ . Update θ by minimizing $\mathcal{L}_{\text{w-CFM}} + \alpha \mathcal{L}_{\text{ent}}$ (Eqs. 9, 15).
- 12: Update α using dual gradient descent.
- 13: Update target networks.
- 14: **end for**
- 15: **end for**

to the divergence of the induced vector field:

$$H_0^a = H_0^x + \mathbb{E}_{x_0 \sim p_0} \left[\sum_{i=1}^d \log(1 - \tanh^2(x_{0,i})) \right], \quad (17)$$

$$H_1^a \approx H_0^a + \mathbb{E}_{t \sim \mathcal{U}[0,1], x_t \sim p_t(\cdot|s)} [\nabla_a \cdot v^a(a, t, s)]. \quad (18)$$

Since H_0^x and the Jacobian expectation in Eq. (17) depend only on the fixed base distribution p_0 , H_0^a is constant w.r.t. the policy parameters θ . Therefore, it can be omitted from the optimization objective without affecting the gradient.

4.4. Training Procedure

The complete procedure is summarized in Algorithm 1. For the value network update, the critic parameters ψ are updated to minimize the Bellman Mean Squared Error (MSE). Given a transition tuple (s_i, a_i, r_i, s_{i+1}) sampled from the replay buffer \mathcal{D} , the loss is defined as:

$$\mathcal{L}_Q(\psi) = \mathbb{E}_{\mathcal{D}} \left[(y_i - Q_\psi(s_i, a_i))^2 \right], \quad (19)$$

where y_i is the regression target constructed using the target networks $\bar{Q}_{\bar{\psi}_1}, \bar{Q}_{\bar{\psi}_2}$. To mitigate value overestimation, we employ the Clipped Double Q-learning mechanism (Fujiimoto et al., 2018):

$$y_i = r_i + \gamma \min_{j=1,2} \bar{Q}_{\bar{\psi}_j}(s_{i+1}, a_{i+1}), \text{ where } a_{i+1} \sim \pi_\theta(\cdot|s_{i+1}). \quad (20)$$

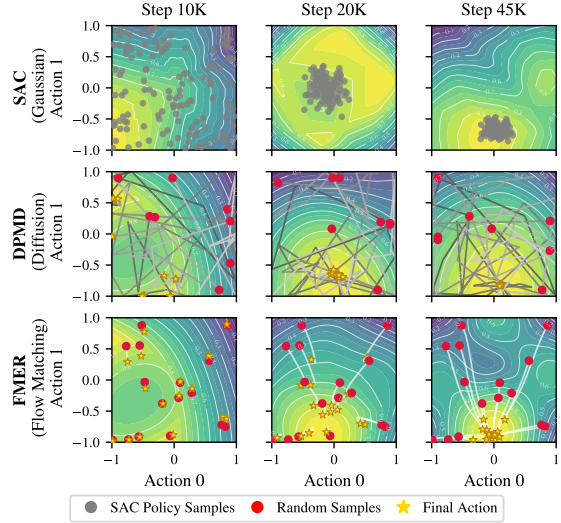


Figure 3. Policy evolution on the 2D multi-goal task for the same state $s = (0, 0)$. Background contours depict the learned critic $Q(s, a)$ over action space. For SAC, points show policy samples, and for the generative policies, red dots show the random noise samples and their sampling trajectory towards the final action.

Previously, we introduced the weighted FM loss for policy optimization, where M actions are sampled to accurately estimate the advantage-weighted objective. For the data collection stage, following the advice of Ding et al. (2024) and Kang et al. (2023), we sample M candidates, select the highest-valued action to interact with the environment, and store the resulting transition in the replay buffer, ensuring the buffer is populated with high-reward transitions. Similarly, for the critic update (Eq. 20), we compute the target using the highest-value candidate to reduce the variance of the Bellman backup.

5. Experiments

In this section, we evaluate FMER across a multigoal environment, FrankaKitchen and MuJoCo benchmarks. We first use two toy tasks to visualize generative trajectories and multimodal behavior, then compare against strong baselines on FrankaKitchen and MuJoCo. We further ablate advantage weighting and entropy regularization, and report runtime and memory overhead.

5.1. Visualizing Stochastic Policies for Multi-Goal

To isolate how different stochastic policy families behave in a multi-modal action landscape, we use the standard 2D *multi-goal* environment commonly adopted for interpretability studies (Haarnoja et al., 2017). We compare SAC (Haarnoja et al., 2018) (Gaussian policy), DPMD (diffusion policy), and FMER (our flow matching policy). Figure 3 visualizes, for the same state $s = (0, 0)$, the action

Table 1. Quantitative results on the FrankaKitchen benchmark across a range of task counts (N). We report both the mean number of accomplished tasks and the success rate (%). Results represent the maximum performance over 1M environment steps, averaged across 5 random seeds, with standard deviation shown in parentheses.

Method	Accomplished Tasks				Success Rate (%)			
	N=1	N=2	N=4	N=7	N=1	N=2	N=4	N=7
PPO	0.02 (0.04)	0.18 (0.40)	0.06 (0.09)	0.78 (0.44)	2.00 (4.47)	9.00 (20.12)	1.50 (2.24)	11.14 (6.26)
SAC	0.80 (0.45)	1.40 (0.34)	1.24 (0.37)	1.22 (0.45)	80.00 (44.72)	70.00 (16.96)	31.00 (9.29)	17.43 (6.42)
TD3	0.00 (0.00)	0.62 (0.57)	0.72 (0.82)	0.92 (0.88)	0.00 (0.00)	31.00 (28.37)	18.00 (20.49)	13.14 (12.51)
FPO	0.18 (0.20)	0.50 (0.47)	0.32 (0.26)	0.66 (0.21)	18.00 (20.49)	25.00 (23.72)	8.00 (6.47)	9.43 (2.96)
DIPO	0.22 (0.44)	0.72 (0.66)	0.94 (0.88)	1.78 (1.11)	22.00 (43.82)	36.00 (33.05)	23.50 (22.12)	25.43 (15.92)
DPMD	0.64 (0.49)	1.12 (0.27)	1.22 (0.44)	1.56 (0.82)	64.00 (49.30)	56.00 (13.42)	30.50 (10.95)	22.29 (11.68)
QVPO	0.02 (0.04)	0.08 (0.13)	0.08 (0.13)	1.48 (0.69)	2.00 (4.47)	4.00 (6.52)	2.00 (3.26)	21.14 (9.87)
FMER	1.00 (0.00)	1.26 (0.32)	2.00 (0.14)	3.20 (1.06)	100.00 (0.00)	63.00 (16.05)	50.00 (3.54)	45.71 (15.08)

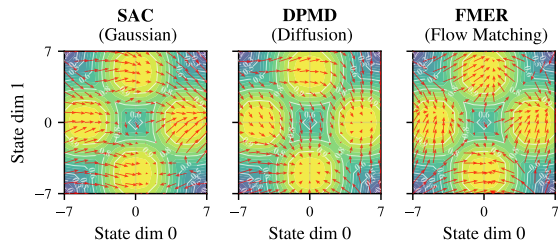


Figure 4. State-conditioned policy visualization on the 2D multi-goal task. Background colors depict the ground-truth state-value landscape, where the four bright regions indicate the optimal goals. Red arrows show the policy-selected action at each state for SAC, DPMD, and FMER. The resulting vector field reveals the navigation strategy of each method.

samples produced by each policy at an early (10K), intermediate (20K), and converged (45K) stage of training. SAC initially concentrates samples in a broad, unimodal region and only gradually shifts mass toward a high-value basin, reflecting the limited ability of a single Gaussian to represent disconnected modes. In contrast, both DPMD and FMER allocate probability mass to the high-value region much earlier, indicating faster discovery of promising modes. Diffusion denoising trajectories are often indirect and vary across samples, whereas FMER induces smoother and more coherent transport toward high-value actions.

Furthermore, Figure 4 illustrates the state-conditioned action selection across the multi-goal environment after training has converged. As shown by the red arrows, SAC and DPMD consistently orient toward a subset of optimal regions (right and bottom), even when alternative peaks are equally optimal. In contrast, FMER adapts to the local geometry and points toward the nearest of the four equal-valued maxima. This indicates a diverse multimodal behavior facilitated by the precise entropy control of our ODE-based formulation.

5.2. Benchmarks on FrankaKitchen and Mujoco

We evaluate FMER against a diverse range of seven reinforcement learning baselines across two continuous control benchmarks: FrankaKitchen (Gupta et al., 2020) and Mu-

JoCo. To provide a comprehensive comparison, our baseline suite spans three distinct algorithmic categories: standard RL algorithms, including PPO (Schulman et al., 2017), SAC (Haarnoja et al., 2018), and TD3 (Fujimoto et al., 2018); recent off-policy diffusion-based methods, specifically DIPO (Yang et al., 2023), QVPO (Ding et al., 2024), and DPMD (Ma et al., 2025); and the flow-matching-based on-policy baseline FPO (McAllister et al., 2026). Detailed baseline implementations and the specific hyperparameters used for FMER are provided in Appendix B.

For all experiments, we report the mean performance across 5 random seeds on 10 environments, each with a budget of 1 million environment interaction steps. For off-policy methods, we include a warm-up phase of 10,000 transitions collected by a random policy. Policies are evaluated every 10,000 steps.

FrankaKitchen The FrankaKitchen benchmark (Gupta et al., 2020) features a 9 degrees of freedom Franka robot situated in a realistic kitchen environment containing several interactable household items such as a microwave, kettle, overhead light, cabinets, and an oven. This environment is inherently sparse; the agent is allotted a maximum of 280 steps per episode and receives a binary reward of 1 only upon the successful completion of a sub-task. Moreover, the environment exhibits a multimodal value distribution because multiple distinct, state-dependent behaviors can lead to high returns, for instance, different sequences of object interactions can satisfy the same goal configuration. To evaluate FMER across different task complexities, we conduct experiments on four configurations with $N \in \{1, 2, 4, 7\}$ tasks. Detailed task compositions and experimental setups are provided in Appendix B.

As demonstrated in Table 1, FMER outperforms all baselines across nearly all task compositions, achieving competitive performance at $N = 2$ and significantly superior results as complexity increases. A general trend across all models is that as N increases, the number of accomplished tasks rises while the overall success rate declines. This occurs because agents can more easily identify and complete isolated, simpler sub-tasks to gain initial rewards; however, the fixed

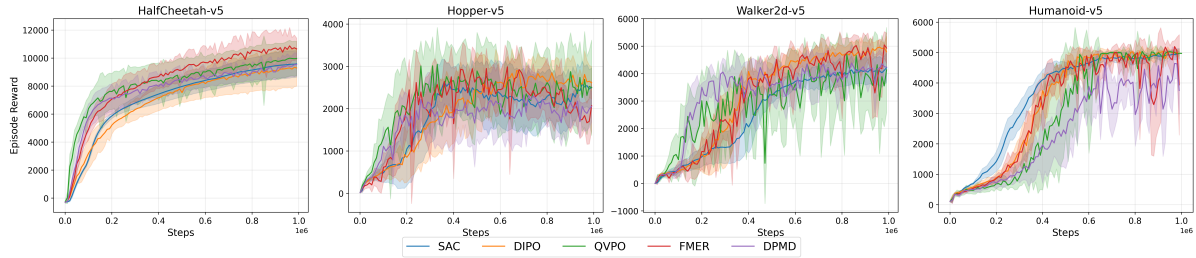


Figure 5. Training curves on four MuJoCo locomotion benchmarks. We report the average episodic return over 5 random seeds, with solid lines representing the mean and shaded regions indicating the standard deviation. For visual clarity, we compare FMER against the four top-performing diffusion baselines (QVPO, DPMD, DIPO, SAC). Curves are smoothed with a 10,000-step window.

Table 2. Evaluation results on MuJoCo benchmarks. We report the maximum average return over 1M environment steps, averaged across 5 random seeds. Values are presented as Mean (Std).

Algorithm	Hopper	HalfCheetah	Walker2d	Humanoid
PPO	1223.19 (345.21)	5982.74 (810.60)	4606.76 (211.17)	811.94 (78.20)
SAC	3354.63 (90.53)	10295.33 (1170.43)	4453.24 (521.33)	5350.96 (75.07)
TD3	3664.30 (60.89)	9496.59 (901.14)	4969.19 (668.54)	363.16 (202.48)
FPO	1216.86 (241.82)	2860.01 (1513.28)	635.33 (219.05)	371.46 (163.38)
DIPO	3592.82 (104.07)	9516.47 (1417.20)	5028.66 (217.36)	5123.38 (78.81)
DPMD	3503.62 (65.09)	10706.06 (817.59)	4910.31 (350.06)	5100.60 (44.91)
QVPO	3671.77 (205.24)	10309.60 (1398.37)	4846.39 (397.71)	5078.00 (47.22)
FMER	3444.46 (158.88)	12332.38 (903.67)	5285.08 (438.80)	5286.12 (65.35)

budget of 280 steps becomes a bottleneck for sequential completion, leaving insufficient steps for later sub-tasks.

Among the baselines, SAC demonstrates the strongest performance for small N due to its explicit use of policy entropy, which facilitates exploration in sparse-reward settings. However, SAC’s performance degrades when transitioning from $N = 2$ to $N = 4$, with the mean number of accomplished tasks decreasing. We attribute this to the increasingly pronounced multimodal nature of the optimal action distribution as task complexity grows, a characteristic that unimodal Gaussian policies are inherently unable to capture.

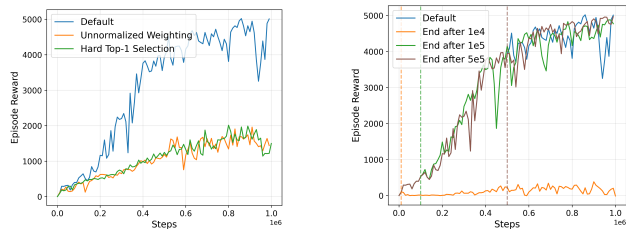
Furthermore, we observe that existing diffusion-based baselines struggle in FrankaKitchen; this is because SDE-based diffusion typically lacks explicit, tractable control over entropy, often resorting to suboptimal heuristics that hinder effective exploration. While the flow-matching-based policy FPO attempts to bridge this gap, it is built upon the PPO framework and uses Flow Matching primarily to calculate the likelihood-ratio surrogate. Consequently, it remains limited because PPO fundamentally lacks explicit control over the policy entropy. In contrast, FMER leverages a flow-matching backbone capable of representing complex, non-Gaussian distributions. By integrating our derived closed-form entropy solution, FMER maintains principled exploration and accurately tracks multimodal targets, leading to superior performance across realistic, sparse-reward multitask environments.

MuJoCo We evaluate FMER on the MuJoCo locomotion suite, which serves as a standard benchmark for continuous control with dense rewards and typically unimodal action distributions. Quantitative results in Table 2 and learning curves in Figure 5 demonstrate that FMER achieves state-of-the-art or highly competitive performance across the benchmark. Notably, FMER secures the highest returns on HalfCheetah-v5 and Walker2d-v5, significantly outperforming all generative and diffusion-based baselines. On the high-dimensional Humanoid-v5 task, FMER surpasses all diffusion-based methods such as DIPO, DPMD, and QVPO, demonstrating its ability to model complex dynamics without the training instabilities common in generative policies. While SAC maintains the highest return on Humanoid-v5, FMER remains the top-performing model within the generative policy class. The learning curves reveal that FMER exhibits a more gradual convergence profile compared to some baselines. This is a principled result of our entropy-constrained optimization: the Lagrangian multiplier α actively enforces exploration during early training, preventing premature collapse into suboptimal modes and ultimately enabling the discovery of higher-reward solutions across different environments.

5.3. Ablation Study

To examine the impact of the policy update strategy and the entropy regularization (\mathcal{L}_{ent}), we conduct ablation experiments using Walker2d-v5 as an example. Sensitivity analysis on advantage-weight τ can be found in Appendix C.

Impact of Advantage Weighting Strategies. In Figure 6a, we evaluate the effectiveness of our multi-candidate advantage-weighted flow matching (Eq. (11)) by comparing it against two alternative strategies: (1) Unnormalized Weighting, where weights are computed directly as $w = \exp(A/\tau)$ without softmax normalization; and (2) Hard Top-1 Selection, where we train exclusively on the single candidate with the highest advantage. We observe that both alternatives lead to premature convergence and suboptimal performance. The unnormalized approach likely fails because it assigns different total weight magnitudes to



(a) Comparison between different weight strategies.

(b) Deactivate \mathcal{L}_{ent} after different step thresholds.

Figure 6. Examining the advantage-based weight strategy and entropy regularization parameters.

different states; in contrast, our softmax normalization ensures the total weight sum per state is constant ($\sum w_i = 1$), guaranteeing a consistent learning signal across the state space. Meanwhile, the Hard Top-1 is not performing well because it lacks robustness against the inaccuracies in value estimation during early training.

Effect of Entropy Regularization. In Figure 6b, we investigate the necessity of entropy regularization by deactivating \mathcal{L}_{ent} after varying step thresholds. We observe that early removal (10^4 steps) causes an immediate performance collapse, an instability exacerbated by the deterministic nature of the ODE-based policy which relies heavily on entropy for initial exploration. However, when removed at an intermediate stage (10^5 steps), the agent successfully converges, albeit with increased fluctuation. This confirms that the weighted Flow Matching loss alone suffices for policy improvement once baseline competence is attained, consistent with Theorem 1. Finally, late-stage removal (5×10^5 steps) results in a smoother training curve than the default setting, as the variance induced by entropy-driven exploration is eliminated during policy refinement.

5.4. Computation and memory cost

Table 3 summarizes the computational overhead of FMER compared to diffusion-based baselines, reporting both GPU memory usage and total training time on Humanoid-v5. All models were trained on a single NVIDIA V100 GPU paired with 5 CPU cores (25GB system RAM). While QVPO achieves strong performance on benchmarks, it requires over 29 hours to finish training. In comparison, FMER achieves a $7\times$ speedup over QVPO and a 10–15% reduction in training time relative to efficient baselines like DIPO and DPMD. FMER also shows superior memory efficiency, achieving a more than $10\times$ reduction in memory footprint compared to QVPO and nearly a 40% reduction compared to DIPO. These results indicate that FMER’s less sampling steps and ODE-based transport offer improved computational efficiency while maintaining good performance.

Table 3. GPU memory allocation and total compute time of 1 million environment interactions on Humanoid-v5.

Algorithm	GPU Memory (MB)	Training time (min)
DIPO (JAX)	722	294
DPMD (JAX)	772	276
QVPO (JAX)	4838	1760
FMER (JAX)	454	247

6. Conclusion

We presented FMER, an ODE-based online RL framework that overcomes the intractability of entropy control in diffusion policies. By combining advantage-weighted flow matching with a tractable entropy objective, FMER enables principled exploration and stable convergence. Experiments demonstrate that FMER outperforms state-of-the-art diffusion methods on complex benchmarks such as FrankaKitchen and is more computationally efficient. Our analysis reveals that explicit entropy regularization is essential for initial exploration, validating the necessity of our ODE-based formulation for avoiding local optima. Despite its efficiency, FMER’s use of a fixed-step Euler solver and a constant target entropy presents limitations in integration accuracy and late-stage refinement. Future work will investigate higher-order solvers and adaptive entropy scheduling. Detailed discussion is provided in Appendix D.

Impact statement

This paper presents work whose goal is to advance the field of Machine Learning. There are many potential societal consequences of our work, none which we feel must be specifically highlighted here.

References

- Ajay, A., Du, Y., Gupta, A., Tenenbaum, J. B., Jaakkola, T. S., and Agrawal, P. Is conditional generative modeling all you need for decision making? In *The Eleventh International Conference on Learning Representations, ICLR 2023, Kigali, Rwanda, May 1-5, 2023*. OpenReview.net, 2023. URL <https://openreview.net/forum?id=sP1fo2K9DFG>.
- Celik, O., Li, Z., Blessing, D., Li, G., Palenicek, D., Peters, J., Chalvatzaki, G., and Neumann, G. DIME: diffusion-based maximum entropy reinforcement learning. In *Forty-second International Conference on Machine Learning, ICML 2025, Vancouver, BC, Canada, July 13-19, 2025*. OpenReview.net, 2025. URL <https://openreview.net/forum?id=Aw6dBR7Vxj>.
- Chen, H., Lu, C., Ying, C., Su, H., and Zhu, J. Offline reinforcement learning via high-fidelity generative behavior modeling. In *The Eleventh International Conference on Learning Representations, ICLR 2023, Kigali, Rwanda, May 1-5, 2023*. OpenReview.net, 2023. URL <https://openreview.net/forum?id=42zs3qa2kpy>.
- Chen, R. T., Rubanova, Y., Bettencourt, J., and Duvenaud, D. K. Neural ordinary differential equations. *Advances in neural information processing systems*, 31, 2018.
- Ding, S., Hu, K., Zhang, Z., Ren, K., Zhang, W., Yu, J., Wang, J., and Shi, Y. Diffusion-based reinforcement learning via q-weighted variational policy optimization. *Advances in Neural Information Processing Systems*, 37: 53945–53968, 2024.
- Fujimoto, S., van Hoof, H., and Meger, D. Addressing function approximation error in actor-critic methods. In *Proceedings of the 35th International Conference on Machine Learning (ICML)*, Proceedings of Machine Learning Research, 2018. URL <https://proceedings.mlr.press/v80/fujimoto18a.html>.
- Grathwohl, W., Chen, R. T. Q., Bettencourt, J., Sutskever, I., and Duvenaud, D. FFJORD: free-form continuous dynamics for scalable reversible generative models. In *7th International Conference on Learning Representations, ICLR 2019, New Orleans, LA, USA, May 6-9, 2019*. OpenReview.net, 2019. URL <https://openreview.net/forum?id=rJxgknCcK7>.
- Gupta, A., Kumar, V., Lynch, C., Levine, S., and Hausman, K. Relay policy learning: Solving long-horizon tasks via imitation and reinforcement learning. In Kaelbling, L. P., Kragic, D., and Sugiura, K. (eds.), *Proceedings of the Conference on Robot Learning*, volume 100 of *Proceedings of Machine Learning Research*, pp. 1025–1037. PMLR, 30 Oct–01 Nov 2020. URL <https://proceedings.mlr.press/v100/gupta20a.html>.
- Haarnoja, T., Tang, H., Abbeel, P., and Levine, S. Reinforcement learning with deep energy-based policies. In *International conference on machine learning*, pp. 1352–1361. PMLR, 2017.
- Haarnoja, T., Zhou, A., Abbeel, P., and Levine, S. Soft actor-critic: Off-policy maximum entropy deep reinforcement learning with a stochastic actor. In *Proceedings of the 35th International Conference on Machine Learning (ICML)*, Proceedings of Machine Learning Research, 2018. URL <https://proceedings.mlr.press/v80/haarnoja18b.html>.
- Ho, J., Jain, A., and Abbeel, P. Denoising diffusion probabilistic models. *Advances in neural information processing systems*, 33:6840–6851, 2020.
- Hutchinson, M. F. A stochastic estimator of the trace of the influence matrix for laplacian smoothing splines. *Communications in Statistics-Simulation and Computation*, 18(3):1059–1076, 1989.
- Kang, B., Ma, X., Du, C., Pang, T., and Yan, S. Efficient diffusion policies for offline reinforcement learning. *Advances in Neural Information Processing Systems*, 36: 67195–67212, 2023.
- Lipman, Y., Chen, R. T. Q., Ben-Hamu, H., Nickel, M., and Le, M. Flow matching for generative modeling. In *The Eleventh International Conference on Learning Representations, ICLR 2023, Kigali, Rwanda, May 1-5, 2023*. OpenReview.net, 2023. URL <https://openreview.net/forum?id=PqvMRDCJT9t>.
- Liu, J., Liu, G., Liang, J., Li, Y., Liu, J., Wang, X., Wan, P., ZHANG, D., and Ouyang, W. Flow-GRPO: Training flow matching models via online RL. In *The Thirty-ninth Annual Conference on Neural Information Processing Systems*, 2025. URL <https://openreview.net/forum?id=oCBKGw5HNf>.
- Ma, H., Chen, T., Wang, K., Li, N., and Dai, B. Efficient online reinforcement learning for diffusion policy. In *Forty-second International Conference on Machine Learning, ICML 2025, Vancouver, BC, Canada, July 13-19, 2025*. OpenReview.net, 2025. URL <https://openreview.net/forum?id=6Anv3KB9lz>.

- McAllister, D., Ge, S., Yi, B., Kim, C. M., Weber, E., Choi, H., Feng, H., and Kanazawa, A. Flow matching policy gradients, 2025. URL <https://arxiv.org/abs/2507.21053>.
- McAllister, D., Ge, S., Yi, B., Kim, C. M., Weber, E., Choi, H., Feng, H., and Kanazawa, A. Flow matching policy gradients. In *The Fourteenth International Conference on Learning Representations*, 2026. URL <https://openreview.net/forum?id=e0EmoKoQpJ>.
- Peng, X. B., Kumar, A., Zhang, G., and Levine, S. Advantage-weighted regression: Simple and scalable off-policy reinforcement learning. *arXiv preprint arXiv:1910.00177*, 2019.
- Psenka, M., Escontrela, A., Abbeel, P., and Ma, Y. Learning a diffusion model policy from rewards via q-score matching. In *Proceedings of the 41st International Conference on Machine Learning, ICML'24*. JMLR.org, 2024.
- Ren, A. Z., Lidard, J., Ankile, L. L., Simeonov, A., Agrawal, P., Majumdar, A., Burchfiel, B., Dai, H., and Simchowitz, M. Diffusion policy optimization. In *The Thirteenth International Conference on Learning Representations, ICLR 2025, Singapore, April 24-28, 2025*. OpenReview.net, 2025. URL <https://openreview.net/forum?id=mEpqHvbD2h>.
- Rouxel, Q., Donoso, C., Chen, F., Ivaldi, S., and Mouret, J. Extremum flow matching for offline goal conditioned reinforcement learning. In *24th IEEE-RAS International Conference on Humanoid Robots, Humanoids 2025, Seoul, Republic of Korea, September 30 - October 2, 2025*, pp. 981–988. IEEE, 2025. doi: 10.1109/HUMANOIDS65713.2025.11203207. URL <https://doi.org/10.1109/Humanoids65713.2025.11203207>.
- Schulman, J., Wolski, F., Dhariwal, P., Radford, A., and Klimov, O. Proximal policy optimization algorithms. *arXiv preprint arXiv:1707.06347*, 2017. URL <https://arxiv.org/abs/1707.06347>.
- Wan, Z., Wu, J., Yu, X., Zhang, C., Lei, M., An, B., and Tsang, I. Fm-irl: Flow-matching for reward modeling and policy regularization in reinforcement learning, 2025. URL <https://arxiv.org/abs/2510.09222>.
- Wang, Y., Wang, L., Jiang, Y., Zou, W., Liu, T., Song, X., Wang, W., Xiao, L., Wu, J., Duan, J., and Li, S. Diffusion actor-critic with entropy regulator. In Globersons, A., Mackey, L., Belgrave, D., Fan, A., Paquet, U., Tomczak, J. M., and Zhang, C. (eds.), *Advances in Neural Information Processing Systems 38: Annual Conference on Neural Information Processing Systems 2024, NeurIPS 2024, Vancouver, BC, Canada, December 10 - 15, 2024*, 2024.
- Wang, Z., Hunt, J. J., and Zhou, M. Diffusion policies as an expressive policy class for offline reinforcement learning. In *The Eleventh International Conference on Learning Representations, ICLR 2023, Kigali, Rwanda, May 1-5, 2023*. OpenReview.net, 2023. URL <https://openreview.net/forum?id=AHvFDPi-FA>.
- Yang, L., Huang, Z., Lei, F., Zhong, Y., Yang, Y., Fang, C., Wen, S., Zhou, B., and Lin, Z. Policy representation via diffusion probability model for reinforcement learning. *CoRR*, abs/2305.13122, 2023. doi: 10.48550/ARXIV.2305.13122. URL <https://doi.org/10.48550/arXiv.2305.13122>.
- Zhang, S., Zhang, W., and Gu, Q. Energy-weighted flow matching for offline reinforcement learning. In *The Thirteenth International Conference on Learning Representations, ICLR 2025, Singapore, April 24-28, 2025*. OpenReview.net, 2025. URL <https://openreview.net/forum?id=HA0oLUvuGI>.
- Zheng, Q., Zhang, A., and Grover, A. Online decision transformer. In Chaudhuri, K., Jegelka, S., Song, L., Szepesvári, C., Niu, G., and Sabato, S. (eds.), *International Conference on Machine Learning, ICML 2022, 17-23 July 2022, Baltimore, Maryland, USA*, volume 162 of *Proceedings of Machine Learning Research*, pp. 27042–27059. PMLR, 2022. URL <https://proceedings.mlr.press/v162/zheng22c.html>.

A. Proofs

A.1. Proof of Theorem 1

Theorem 1 (Weighted Flow Matching Surrogate). For a given state s and advantage weights $w(s, a) = \exp(A(s, a)/\tau)$, let $x_1 = \operatorname{arctanh}(a)$ be the action mapped to the unbounded latent space. Minimizing the Weighted Conditional Flow Matching loss:

$$\mathcal{L}_{\text{W-CFM}}(\theta) = \mathbb{E}_{\substack{t \sim \mathcal{U}[0,1] \\ a \sim \pi_k(\cdot|s) \\ x_0 \sim p_0}} \left[w(s, a) \|v_\theta(x_t, t, s) - (x_1 - x_0)\|^2 \right] \quad (21)$$

is a surrogate for maximizing the lower bound of the advantage-weighted policy improvement objective:

$$\mathbb{E}_{s, a \sim \pi_k(\cdot|s)} [w(s, a) \log \pi_\theta(a|s)]. \quad (22)$$

Proof. We formulate Flow Matching in a latent variable framework. Let x denote the latent state and $a = \tanh(x_1)$ the action. We utilize a reverse process p_θ (generative, Noise \rightarrow Latent Target) and a forward process q (Latent Target \rightarrow Noise). We define time $t \in [0, 1]$. Although Flow Matching is typically treated as a deterministic ODE, for the purpose of this derivation (to ensure the KL divergence is well-defined), we model the path transitions as Gaussian distributions with variance $\sigma^2 \Delta t$ and $\Delta t \rightarrow 0$.

Continuous Flow Matching Framework. For a continuous-time flow with time discretization Δt , the learned generative transition (p_θ) evolves forward in time:

$$x_{t+\Delta t} = x_t + v_\theta(x_t, t, s) \Delta t. \quad (23)$$

Modeled as a Gaussian step, this transition probability is:

$$p_\theta(x_{t+\Delta t}|x_t, s) = \mathcal{N}(x_{t+\Delta t}; x_t + v_\theta(x_t, t, s) \Delta t, \sigma^2 \Delta t \mathbf{I}). \quad (24)$$

To define the objective, we construct the target conditional probability path q . Given a noise sample x_0 and a target latent state $x_1 = \operatorname{arctanh}(a)$, we use the Optimal Transport linear interpolation. The conditional target distribution is locally defined as:

$$q(x_t|x_0, x_1) = \mathcal{N}(x_t; (1-t)x_0 + tx_1, \sigma_q^2 \mathbf{I}), \quad x \sim p_0, \quad (25)$$

where $\sigma_q \rightarrow 0$ represents the noise floor of the target path.

Decomposition of Log-Likelihood. By the change of variables formula, $\log \pi_\theta(a|s) = \log p_\theta(x_1|s) + \log |\det J(a)|$. Since the Jacobian term depends only on a and not θ , maximizing $\log \pi_\theta(a|s)$ is equivalent to maximizing $\log p_\theta(x_1|s)$. We proceed by marginalizing over the latent trajectory $x_{0:1-\Delta t}$:

$$\log p_\theta(x_1|s) = \log \int p_\theta(x_{0:1}|s) dx_{0:1-\Delta t} \quad (26)$$

$$= \log \int \frac{p_\theta(x_{0:1}|s)}{q(x_{0:1-\Delta t}|x_1, x_0)} q(x_{0:1-\Delta t}|x_1, x_0) dx_{0:1-\Delta t} \quad (27)$$

$$= \log \mathbb{E}_{x_{0:1-\Delta t} \sim q(\cdot|x_1, x_0)} \left[\frac{p_\theta(x_{0:1}|s)}{q(x_{0:1-\Delta t}|x_1, x_0)} \right] \quad (28)$$

By Jensen's inequality (concavity of \log):

$$\log p_\theta(x_1|s) \geq \mathbb{E}_q \left[\log \frac{p_\theta(x_{0:1}|s)}{q(x_{0:1-\Delta t}|x_1, x_0)} \right] = \text{ELBO}(x_1, s). \quad (29)$$

Weighted ELBO. Since $w(s, a) = \exp(\frac{A(s, a)}{\tau}) \geq 0$, maximizing the weighted ELBO maximizes a lower bound on the policy improvement objective:

$$\mathbb{E}_{a \sim \pi_k} [w(s, a) \log p_\theta(x_1|s)] \geq \mathbb{E}_{a \sim \pi_k} [w(s, a) \cdot \text{ELBO}(x_1, s)]. \quad (30)$$

Connection between ELBO and FM loss. Factorizing the numerator p_θ and the denominator q inside the ELBO gives:

$$\text{ELBO} = \mathbb{E}_q \left[\sum_t \log p_\theta(x_{t+\Delta t} | x_t, s) \right] + \mathbb{E}_q [\log p_0(x_0)] - \mathbb{E}_q [\log q(x_{0:1-\Delta t} | x_1, x_0)] \quad (31)$$

$$= \mathbb{E}_q \left[\sum_t \log p_\theta(x_{t+\Delta t} | x_t, s) \right] + C \quad (32)$$

where C collects terms independent of θ . Expanding the Gaussian log-density from Eq. (24):

$$\log p_\theta(x_{t+\Delta t} | x_t, s) \propto -\frac{1}{2\sigma^2\Delta t} |x_{t+\Delta t} - x_t - v_\theta(x_t, t, s)\Delta t|^2. \quad (33)$$

Substituting Eq. (33) into the ELBO, and noting that under the target distribution q , the transition is $x_{t+\Delta t} \approx x_t + u_t^{\text{target}}\Delta t$ with $u_t^{\text{target}} = x_1 - x_0$:

$$\text{ELBO} \approx -\frac{1}{2\sigma^2} \mathbb{E}_q \left[\sum_t |(x_1 - x_0) - v_\theta(x_t, t, s)|^2 \Delta t \right] + C. \quad (34)$$

Since Δt and σ are constants, maximizing the ELBO corresponds to minimizing the Flow Matching loss:

$$\text{ELBO} \approx -\frac{1}{2\sigma^2} \mathcal{L}_{\text{FM}}(\theta) + C, \quad \mathcal{L}_{\text{FM}}(\theta) = \mathbb{E}_{t,q} [|v_\theta(x_t, t, s) - (x_1 - x_0)|^2]. \quad (35)$$

Since $\sigma^2 > 0$ is a constant independent of θ , multiplying the objective function by the positive scalar $1/\sigma^2$ scales the magnitude of the gradients but does not change the location of the global minimum in the parameter space. Consequently, the optimal parameters θ^* that minimize the Flow Matching loss are identical to those that maximize the ELBO. Thus, minimizing the flow matching loss is a valid surrogate for maximizing the lower bound of the RL objective. \square

A.2. Proof of Theorem 2

Theorem 2 (Entropy of Latent Flow). Consider a latent vector field $v_\theta(x, t, s)$ that transports a base distribution p_0 to the target latent distribution p_1 at $t = 1$. For the unbounded latent space \mathbb{R}^d , the entropy $H^x(p_1(\cdot|s))$ can be computed as:

$$H_1^x(p_1) = H_0^x + \int_0^1 \mathbb{E}_{x_t \sim p_t(\cdot|s)} [\nabla_x \cdot v_\theta(x_t, t, s)] dt, \quad (36)$$

where $H_0^x = \frac{d}{2}(1 + \ln(2\pi))$ is the entropy of the base Gaussian noise $p_0 = \mathcal{N}(0, \mathbf{I})$ and d is the latent dimension.

Proof. For simplicity, we use H_t to denote H_t^x in this proof. For all $x \in \mathbb{R}^d$ and $t \in [0, 1]$, a flow model with vector field v_t and probability path $p_t(x)$ satisfies the continuity equation:

$$\frac{\partial p_t}{\partial t} = -\nabla \cdot (p_t v_t). \quad (37)$$

The entropy of the distribution p_t is defined as:

$$H_t = -\int p_t(x) \log p_t(x) dx. \quad (38)$$

Taking the time derivative:

$$\frac{d}{dt} H_t = -\int \left(\log p_t(x) \frac{\partial p_t(x)}{\partial t} + \frac{\partial p_t(x)}{\partial t} \right) dx. \quad (39)$$

Since $\int p_t(x) dx = 1$, the second term vanishes:

$$\frac{d}{dt} H_t = -\int \log p_t(x) \frac{\partial p_t(x)}{\partial t} dx. \quad (40)$$

Substituting Eq. (37) into the expression:

$$\frac{d}{dt}H_t = \int \log p_t(x) \nabla \cdot (p_t v_t) dx. \quad (41)$$

Assuming the probability mass vanishes at the boundaries, we apply integration by parts. Note that $\nabla \log p_t = \frac{\nabla p_t}{p_t}$:

$$\frac{d}{dt}H_t = - \int v_t \cdot \nabla p_t dx. \quad (42)$$

Using the identity $\nabla \cdot (p_t v_t) = p_t \nabla \cdot v_t + v_t \cdot \nabla p_t$ and the integration by parts:

$$\frac{d}{dt}H_t = \int p_t \nabla \cdot v_t dx. \quad (43)$$

Therefore,

$$\frac{d}{dt}H_t = \mathbb{E}_{x \sim p_t} [\nabla \cdot v_t]. \quad (44)$$

Integrating over time from $t = 0$ to $t = 1$:

$$H_1 = H_0 + \int_0^1 \mathbb{E}_{x \sim p_t} [\nabla \cdot v_t] dt. \quad (45)$$

Finally,

$$H_1 = H_0 + \mathbb{E}_{t \sim \mathcal{U}[0,1], x \sim p_t} [\nabla \cdot v_t]. \quad (46)$$

□

A.3. Proof of Proposition 3

Proposition 3 (Divergence under Tanh Transformation). Consider the coordinate transformation $a = \tanh(x)$ mapping any latent state $x \in \mathbb{R}^d$ to the bounded action space $(-1, 1)^d$. Let $v_\theta(x, t, s)$ be the vector field in the latent space. The corresponding induced vector field in the action space, $v^a(a, t, s)$, satisfies the following divergence relationship at any point x :

$$\nabla_a \cdot v^a(a, t, s) = \nabla_x \cdot v_\theta(x, t, s) - \sum_{i=1}^d 2 \tanh(x_i) v_{\theta,i}(x, t, s), \quad (47)$$

where $v_{\theta,i}$ is the i -th component of the latent vector field.

Proof. Theorem 2 assumes an unbounded integration domain where boundary terms vanish. For bounded actions, we consider the domain $a \in (-1, 1)^d$. We employ a change of variables where $a = \tanh(x)$ and the Flow Matching is performed in the unconstrained latent space $x \in \mathbb{R}^d$. The relationship between the velocity fields $v^a(a)$ in the action space and $v_\theta(x)$ in the latent space is given by the chain rule:

$$v_t^a(a) = \frac{da}{dt} = \frac{da}{dx} \frac{dx}{dt} = (1 - a^2) \odot v_\theta(x, t, s). \quad (48)$$

Note that here $(1 - a^2)$ acts element wise. The divergence in the action space is:

$$\nabla_a \cdot v_t^a(a) = \nabla_a \cdot ((1 - a^2) \odot v_\theta(x)). \quad (49)$$

Using the product rule for divergence $\nabla \cdot (f \mathbf{v}) = \nabla f \cdot \mathbf{v} + f \nabla \cdot \mathbf{v}$:

$$\nabla_a \cdot v_t^a(a) = \sum_{i=1}^d \left(v_{\theta,i}(x) \frac{\partial(1 - a_i^2)}{\partial a_i} + (1 - a_i^2) \frac{\partial v_{\theta,i}(x)}{\partial a_i} \right). \quad (50)$$

The first term simplifies to $-2a_i v_{\theta,i}(x)$. For the second term, applying the chain rule yields:

$$\frac{\partial v_{\theta,i}(x)}{\partial a_i} = \frac{\partial v_{\theta,i}(x)}{\partial x_i} \frac{\partial x_i}{\partial a_i} = \frac{\partial v_{\theta,i}(x)}{\partial x_i} \frac{1}{1 - a_i^2}. \quad (51)$$

Substituting Eq. (51) back into Eq. (50), the term $(1 - a_i^2)$ cancels out:

$$\nabla_a \cdot v_t^a(a) = \sum_{i=1}^d \left(-2a_i v_{\theta,i}(x) + \frac{\partial v_{\theta,i}(x)}{\partial x_i} \right) = \nabla_x \cdot v_{\theta}(x) - \sum_{i=1}^d 2a_i v_{\theta,i}(x). \quad (52)$$

This confirms the relationship stated in Proposition 3. □

B. Experiment setup

B.1. Baseline implementation

We use the following codebases for the baseline implementations. Hyperparameters are set according to the specifications in their respective papers; otherwise, the default values are used.

- PPO: <https://stable-baselines3.readthedocs.io/en/master/modules/ppo.html>
- SAC: <https://stable-baselines3.readthedocs.io/en/master/modules/sac.html>
- TD3: <https://stable-baselines3.readthedocs.io/en/master/modules/td3.html>
- DIPO: https://github.com/mahaitongdae/diffusion_policy_online_rl/tree/main
- QVPO: <https://github.com/wadx2019/qvpo/tree/main/agent>
- DPMD: https://github.com/mahaitongdae/diffusion_policy_online_rl/tree/main
- FPO: <https://github.com/akanazawa/fpo>

Table 4. Hyperparameters used in the baselines. *4 for critic update, 32 for evaluation, 64 for actor update.

Hyperparameters	DIPO	DPMD	QVPO	FPO	SAC	TD3	PPO
No. of hidden layers	3	3	2	4	2	2	2
No. of hidden nodes	256	256	256	32	256	256	256
Activation	mish	mish	mish	silu	ReLU	ReLU	ReLU
Batch size	256	256	256	2048	256	256	256
Discount for reward γ	0.99	0.99	0.99	0.99	0.99	0.99	0.99
Reward scale	0.2	0.2	1	1	1	1	1
Target smoothing coefficient	0.005	0.005	0.005	N/A	0.005	0.005	N/A
Learning rate for actor	3×10^{-4} , annealing to 5×10^{-4}		3×10^{-4}	3×10^{-4}	3×10^{-4}	1×10^{-3}	3×10^{-4}
Learning rate for critic	3×10^{-4}	3×10^{-4}	3×10^{-4}	3×10^{-4}	3×10^{-4}	1×10^{-3}	3×10^{-4}
Diffusion steps	100	20	20	10	N/A	N/A	N/A
Candidate set size	1	32	4/32/64*	8	N/A	N/A	N/A

B.2. FMER hyperparameters

Table 5. Hyperparameters used in FMER (shared across all environments).

Hyperparameters	Value
No. of hidden layers	3
No. of hidden nodes	256
Activation	mish
Batch size	256
Discount for reward γ	0.99
Target smoothing coefficient	0.005
Shared learning rate for actor	3×10^{-4} , annealing to 5×10^{-4}
Learning rate for critic	3×10^{-4}
Advantage weight initialized τ	0.5
ODE steps	10
Candidate set size	8

B.3. FrankaKitchen task compositions

The environment details are available at https://robotics.farama.org/envs/franka_kitchen/.

Table 6. FrankaKitchen task compositions.

Tasks (N)	Composition
$N = 1$	“light switch”
$N = 2$	“light switch”, “slide cabinet”
$N = 4$	“light switch”, “slide cabinet”, “bottom burner”, “microwave”
$N = 7$	“light switch”, “slide cabinet”, “bottom burner”, “microwave”, “kettle”, “top burner”, “hinge cabinet”

C. Sensitivity analysis on advantage-weight τ

Figure 7 shows the impact of advantage-weight τ in FMER’s learning process for the Hopper-v5 environment, averaged over 5 seeds. FMER reaches a higher reward around 300K steps when using lower τ values, whereas it explores more gradually when using higher τ values ($\tau = 0.4$).

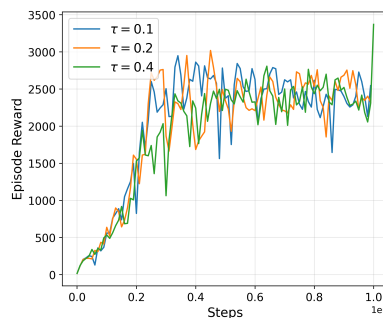


Figure 7. Training curves of different τ values in Hopper-v5.

D. Limitation and future work

Despite the advantages of FMER, it has two primary limitations. First, the use of a fixed-step ODE solver (Euler method) for action sampling introduces a trade-off between integration accuracy and computational speed. Second, the framework currently assumes a fixed target entropy \bar{H} for the dual update of α . As suggested by our ablation studies, α could be adjusted more adaptively across different training stages to better balance initial mode discovery and late-stage policy refinement. Furthermore, such an adaptive α could potentially alleviate the sensitivity of the advantage temperature τ , which currently requires environment-specific tuning. Future work will explore higher-order solvers and adaptive entropy scheduling to further optimize these aspects.